

Microstructural and Mechanical Characterization of a Dissimilar Friction Stir-Welded AA5083-AA7B04 Butt Joint

Yu Chen, Hua Ding, Zhihui Cai, Jingwei Zhao, and Jizhong Li

(Submitted May 26, 2016; in revised form September 11, 2016; published online December 20, 2016)

Friction stir welding (FSW) has been used for joining AA5083 and AA7B04 alloy sheets with the aim of studying the microstructure and the mechanical properties of dissimilar FSW joints obtained by varying the initial base metal state of AA7B04 alloy. The results show that the initial base metal state has a significant impact on the material flow during dissimilar FSW. As compared with the joints placing hard alloy (artificially aged AA7B04-AA or naturally aged AA7B04-NA) on the retreating side, it becomes easier transporting AA5083 from advancing side to retreating side when soft alloy (annealed AA7B04-O) is placed on the retreating side. The atomic diffusion does not occur at the interface between AA5083 and AA7B04, indicating that the mixing of the two materials is merely mechanical. Grain refinement is observed in the stir zone. The failure location during tensile tests is different depending on the initial base metal state. The joints (AA5083/AA7B04-AA and AA5083/AA7B04-O) fail in the base metal on the soft material side which corresponds to the minimum values in hardness profiles. Differently, the joints (AA5083/AA5083 and AA5083/AA7B04-O) fail in the stir zone due to the presence of defects including “zigzag line,” kissing bond and discontinuous voids.

Keywords aluminum alloy, dissimilar joint, friction stir welding, microstructure, mechanical properties

1. Introduction

Friction stir welding (FSW) was invented as a solid-state joining technique at The Welding Institute (TWI) of UK in 1991, and now it has demonstrated great potential in joining materials that are traditionally considered to be unweldable or difficult to weld (Ref 1, 2). In FSW, a rotational tool is plunged into the abutting edges of the two welded plates and traverses along the abutting line, and then, the joints are created. Heat is generated from the friction between the tool and the workpiece and as well as the plastic deformation of the workpiece (Ref 3). Since its development, FSW has been widely and successfully applied in joining similar materials. Besides, FSW can also be used to assemble dissimilar materials. This type of joint is present in a large amount of industrial sectors where fusion welding is usually inappropriate due to the incompatible properties of the components to be welded (such as mechanical behavior, thermal diffusivity or chemical composition) (Ref 4). This is the reason why the application of FSW to different alloy structures raises opportunities. Indeed, joining of dissimilar

materials is very attractive for many applications as we can use the more costly one only where necessary.

A number of studies on FSW of dissimilar materials have been reported. Guo et al. (Ref 5) attempted to join 6.3-mm-thick AA6061 and AA7075 alloys using FSW, examined the effects of material position and welding speed on the microstructure and mechanical properties of the joint, and reported that the material mixing was much more effective when AA6061 alloy was located on the advancing side. Moreover, the highest joint strength was obtained when welding was conducted with the highest welding speed. Rodriguez et al. (Ref 6) researched the impact of tool rotational speed on the microstructure and mechanical properties of dissimilar friction stir-welded 5-mm-thick AA6061-T6 and AA7050-T7451 alloys. An increase in the joint strength was observed with increase in the tool rotational speed. Furthermore, two modes of failure were detected, with one through the stir zone (SZ) at a low rotational speed and the other through the heat-affected zone (HAZ) on the 6061 alloy side at a high rotational speed. Palanivel et al. (Ref 7) stated that pin profile considerably influenced the tensile strength of the dissimilar friction stir-welded AA5083-H111 and AA6351-T6 joints. The joint which was fabricated using straight square pin profile yielded the highest tensile strength. As mentioned above, it can be seen that most of the work merely focuses on the critical process parameters, including the tool geometry, rotational speed, welding speed and the material position. However, to the best of the authors' knowledge, the influence of initial base metal state on the dissimilar FSW behavior has not been well reported so far. Furthermore, based on our previous study (Ref 8), the initial base metal state has a great influence on the microstructure and mechanical properties of similar FSW/FSP samples, and hence, it is necessary to conduct this topic on dissimilar FSW because the material flow and microstructural

Yu Chen, Hua Ding, and Zhihui Cai, School of Materials Science and Engineering, Northeastern University, Shenyang 110819, People's Republic of China; Jizhong Li, School of Mechanical, Materials and Mechatronic Engineering, University of Wollongong, Wollongong, NSW 2522, Australia; and Jingwei Zhao, AVIC Beijing Aeronautical Manufacturing Technology Research Institute, Beijing 100024, People's Republic of China. Contact e-mails: rainy11@126.com and hding2013@163.com.

evolution are much more complex compared with those of similar FSW.

Both AA5083 (Al-Mg alloy) and AA7B04 (Al-Zn-Mg-Cu alloy) have been widely used in aerospace and transportation industries because of their low density and high strength-to-weight ratio. As one of the solution-strengthened alloys, AA5083 can be strengthened by work hardening and grain refinement (Ref 9, 10), presenting excellent corrosion resistance and good formability. AA7B04 is a precipitation-hardened aluminum alloy, demonstrating light weight and high strength (Ref 8). Moreover, different heat treatment states have been developed for AA7B04 over the years, and each state provides the alloy with different performances. Welding AA5083-AA7B04 butt joint is very attractive as we can utilize not only the excellent corrosion resistance of AA5083 but also the high strength of AA7B04. However, on account of the different performances of AA7B04 under different states, the dissimilar FSW behavior on AA5083-AA7B04 butt joint can differ. In the present work, the effect of initial base metal state on the microstructural evolution, Vickers hardness and tensile properties of the dissimilar friction stir-welded AA5083-AA7B04 butt joint were systematically investigated. The present study aims to obtain sound FSW joints with excellent mechanical properties by adjusting the initial base metal temper of AA7B04.

2. Experimental

The base materials used in this study were rolled plates of AA5083 and AA7B04 Al alloys (the thickness is 2 mm). The nominal chemical compositions of these two alloys are listed in Table 1. The rolled AA5083 in the present work was in a partially hardened condition (Ref 11). In addition, three heat treatments of artificial aging (AA), natural aging (NA) and annealing (O) were adopted for AA7B04 alloy. AA heat treatment involved a combination of solution treatment at 480 °C for 80 min followed by water quenching and subsequent artificial aging at 165 °C for 8 h. NA heat treatment was conducted by solution treatment at 480 °C, soaking for 80 min followed by water quenching and aging at ambient temperature for 90 days. O heat treatment comprised of initial heating to 400 °C, soaking for 1 h, followed by furnace cooling to 150 °C and finally air cooling down to ambient temperature. AA7B04 samples applied for the above three heat treatments were designated in three brief forms of AA7B04-AA, AA7B04-NA and AA7B04-O, respectively. The butt FSW was performed parallel to the rolling direction of the plates, with AA5083 being placed on the advancing side (AS) during dissimilar FSW. The detailed information of the experimental process is shown in Table 2. A H13 steel tool with a concave shoulder of 10 mm in diameter and a threaded and tapered pin (diameters of the root and head are 3.9 mm and 1.9 mm, respectively, and the length of the pin is 1.9 mm) was used. The FSW was performed with a rotational speed of 600 rpm and a welding speed of 150 mm/min.

Table 1 Nominal chemical compositions (wt.%) of the studied AA5083 and AA7B04 aluminum alloys

| Alloy | Mg | Zn | Cu | Mn | Fe | Cr | Al |
|--------|---------|------|------|---------|---------|----------|-----|
| AA5083 | 4.4-4.7 | <0.1 | <0.1 | 0.4-0.7 | 0.1-0.2 | 0.1-0.2 | Bal |
| AA7B04 | 2.2 | 6.0 | 1.6 | 0.3 | 0.1 | 0.1-0.25 | Bal |

Microstructure of the cross section of FSW sample was characterized using Olympus DSX-500 optical microscopy (OM), electron back-scattered diffraction (EBSD), scanning electron microscopy (SEM) and transmission electron microscopy (TEM). The samples for OM were ground and polished and then etched using Keller's reagent (190 ml water, 2 ml hydrofluoric acid, 3 ml hydrochloric acid and 5 ml nitric acid). The EBSD analysis was conducted using a FEI Quanta 600 field emission gun scanning electron microscope (FEG-SEM) equipped with TSL OIM™ software, the scanning step of EBSD analysis was 0.2 μm, and the scanning area was 2500 μm². Thin foils for TEM observation, cut from the base metal (BM) and the SZ using an electrical discharge machine, were prepared by jet electro-polishing with a solution of 70% methanol and 30% nitric acid at -30 °C and 19 V. The TEM study was performed on a Tecnai G220 TEM.

The mechanical properties of the FSW samples were evaluated by Vickers hardness and tensile tests. The Vickers hardness measurement was carried out along the centerline of the cross section of FSW sample with a distance between neighboring measured points of 0.5 mm under a load of 50 g for 10 s. Room temperature tensile tests were conducted on a universal testing machine with strain rate of $1 \times 10^{-3} \text{ s}^{-1}$, namely 2.4 mm/min. The specification for the tensile specimen used is Chinese national standard GB/T 228-2002, which is equal to ISO 6892:1998. The transverse tensile specimens were cut perpendicular to the welding direction with a gauge length of 40 mm and a width of 10 mm which covered the SZ, thermo-mechanically affected zone (TMAZ), heat-affected zone (HAZ) and BM, measuring the joint strength. The upper and lower surfaces of all the tensile specimens were mechanically polished to achieve a uniform thickness and to prevent the surface defects from affecting the tensile properties of the samples. The dimensions of the tensile specimen are indicated in Fig. 1, the cross section dimension of the transverse tensile specimen is 10 mm wide and 1.9 mm thickness.

3. Results and Discussion

3.1 Macrostructure

Figure 2 shows the macrostructures of cross section of the joints produced under different FSW conditions. For the similar FSW sample S-1 (Fig. 2a), "zigzag line" is distinctly visible in

Table 2 Experimental process parameters combination

| FSW Joint AS/RS | Designation in brief | Rotational Speed, rpm | Welding Speed, mm/min |
|------------------|----------------------|-----------------------|-----------------------|
| AA5083/AA5083 | S-1 | 600 | 150 |
| AA5083/AA7B04-AA | D-1 | | |
| AA5083/AA7B04-NA | D-2 | | |
| AA5083/AA7B04-O | D-3 | | |

the middle and upper parts of the SZ, and meanwhile, the appearance of the “kissing bond” is detected in the root of the SZ. The zigzag line is sometimes observed in friction stir butt welds, being conventionally attributable to the oxides inherent to the original butt surfaces, and Sato et al. (Ref 12) also suggest that the zigzag line is the remnant of the oxide layer. The SEM image of the kissing bond is shown in Fig. 3. At a relatively low-rotational-speed condition (600 rpm in this study), the original oxide layer is found to be not completely destroyed and a continuous oxide film developed at the root of the SZ, leading to the formation of kissing bond.

For the dissimilar FSW samples (Fig. 2b-d), the AA5083 is positioned on the AS (left-hand side), while the AA7B04 is placed on the opposite or rather the retreating side (RS). Due to the differences in etching response, the AA5083 appears as bright colored regions, whereas the AA7B04 is indicated by the dark colored regions. No void defects are noticeable in the SZ, and the “onion ring” which is often observed in the FSW process is absent (Ref 13, 14). The intermixing of the two materials is also absent. However, parts of the AA5083 materials on the AS penetrate into the RS. Decreasing the strength of AA7B04 (from AA to O state), more AA5083 in the AS transports to the RS, namely AA7B04 side. As illustrated in Table 3, the strength of AA7B04-AA and AA7B04-NA is much higher than that of AA5083, while AA7B04 under O

state is softer than AA5083. For D-1 and D-2 samples, the soft material is AA5083, placing in the AS. It becomes difficult for AA5083 to transport to RS because the flow stress of materials on the RS side (AA7B04-AA and AA7B04-NA) is much higher. It is also reported that less efficient material mixing was obtained when the soft materials was in the AS (Ref 5). On the

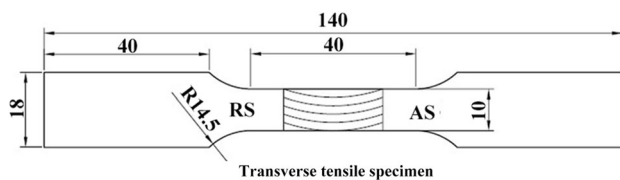


Fig. 1 Dimension of tensile test specimen (all dimensions are in mm)

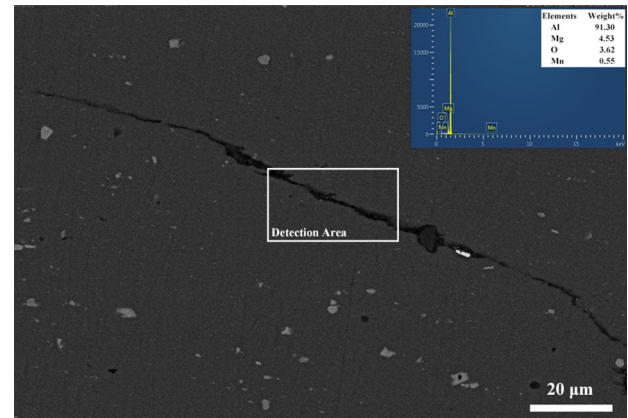


Fig. 3 SEM micrograph of the kissing bond observed in the SZ of sample S-1

Table 3 Mechanical properties of base metal from tensile tests

| Sample | Yield strength, MPa | Ultimate tensile strength, MPa | Elongation, % |
|-----------|---------------------|--------------------------------|---------------|
| AA5083 | 160 ± 1 | 320 ± 0 | 12.3 ± 0.2 |
| AA7B04-AA | 525 ± 5 | 578 ± 3 | 11.3 ± 1.2 |
| AA7B04-NA | 368 ± 3 | 563 ± 2 | 20.8 ± 0.7 |
| AA7B04-O | 110 ± 5 | 220 ± 3 | 20.5 ± 0.5 |

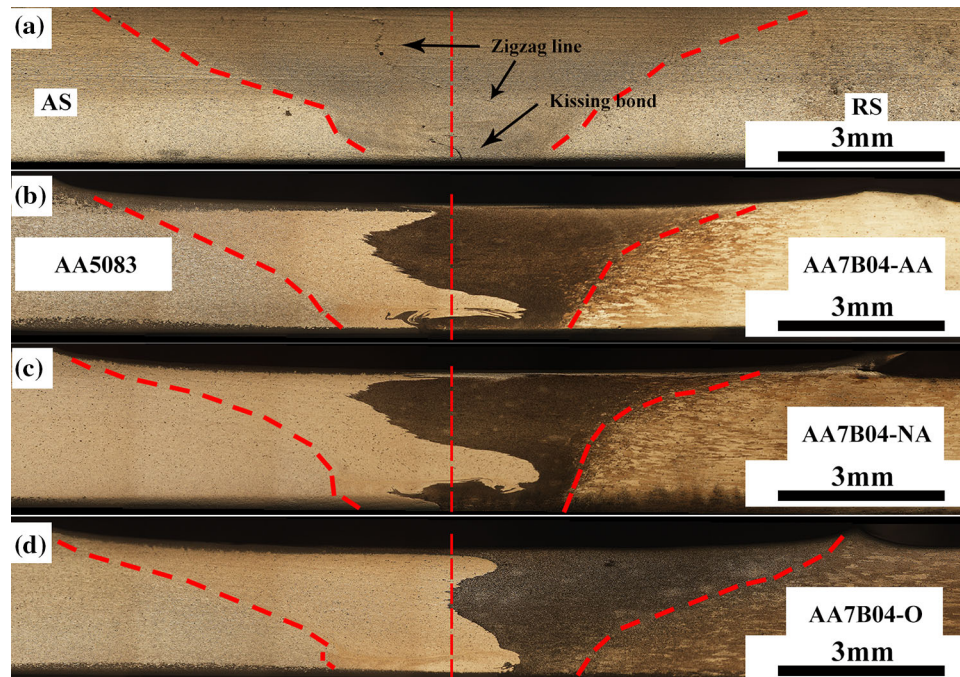


Fig. 2 Low-magnification OM of transversal cross section of FSW samples produced under different conditions (a) similar FSW sample S-1 and dissimilar FSW samples (b) D-1, (c) D-2 and (d) D-3

contrary, the soft material is AA7B04-O for D-3 sample, and hence, the transporting of AA5083 becomes easier. Therefore, it can be concluded that the material flow is different when dissimilar FSW is conducted under different initial BM states.

In addition, an energy-dispersive spectroscopy (EDS) map illustrated in Fig. 4 shows the difference in Mg, Zn, Cu contents of the two sides, displaying the element distribution in the SZ. Based on this map, the left part contains a much higher amount of Mg on the AA5083 side, while a higher amount of Zn and Cu atoms is detected on the AA7B04 side. It indicates that the atomic diffusion does not occur at the interface of AA5083/AA7B04 and the mixing of the two materials is merely mechanical.

3.2 Microstructure

Figure 5(a) shows the microstructure of the AA5083 BM, which comprises coarse grains. The second-phase particles in Al-5083 (Ref 15) are mainly rich in stable Fe and Mn which are difficult to dissolve, and the feature of these particles is irregular as shown in Fig. 6(a). For the AA7B04 BM (Fig. 5b-d), the difference in the morphology of grains is insignificant among AA, NA and O states, where all the microstructure primarily consists of elongated grains. From the results of SEM (in back-scattering electron mode, BSE), it can be seen that the strengthening precipitates are embedded in the Al matrix, and furthermore, the amount of coarse precipitates in AA7B04-AA (Fig. 6b) and AA7B04-NA (Fig. 6c) is less than that in AA7B04-O (Fig. 6d).

The TEM image of AA5083 BM is shown in Fig. 7(a). It can be found that the microstructure is relatively simple in which the second-phase Fe-Mn particles distribute in the Al matrix. Unlike AA5083, the microstructure of AA7B04 under

AA state is more complex (Fig. 7b), and besides the coarse Fe-Mn particles, a high density of particles on the order of 5-10 nm disperses uniformly throughout the matrix. The selected area diffraction pattern (SADP) indicates these fine particles are the strengthening precipitates, η (η')-MgZn₂ phase, which forms during artificial aging. The phase η and η' will not be distinguished in the present work, because it has been reported that the strained version between η' -phase and η -phase was slight (Ref 16). Differently, the fine η (η')-MgZn₂ phase is not detected in AA7B04-NA (Fig. 7c). Under a NA heat treatment, the strengthening precipitates firstly dissolve during solution heat treatment and then the Guinier-Preston (GP) zones precipitate at room temperature (Ref 17-19); however, it is hard to discern GP zones here on account of their fine features and coherent relationship to the matrix. The strengthening precipitates η (η') of 7B04 under O state grow and become much coarser than those under AA and NA states (Fig. 7d), attributing to both the lower cooling speed and longer heating period of annealing.

FSW drastically changes the microstructure in the SZ, including the grain size and the morphology of the second-phase particles (such as Fe-Mn phase and strengthening precipitates η (η') phase). For the similar FSW sample S-1, three aspects can be concluded in the SZ compared with its corresponding BM. Firstly, the fine equiaxed grains resulting from the dynamic recrystallization (DRX) take the place of the initial coarse grains (Fig. 8a). Secondly, the coarse irregular second-phase particles are broken by the stirring of the tool (Fig. 8b). Thirdly, the initial fine particles with a mean diameter of only 100 nm which cannot be broken by the stirring remain unchanged (Fig. 8c). During dissimilar FSW, it becomes interesting to determine whether any interference exists between AA5083 and AA7B04 that may lead to a different

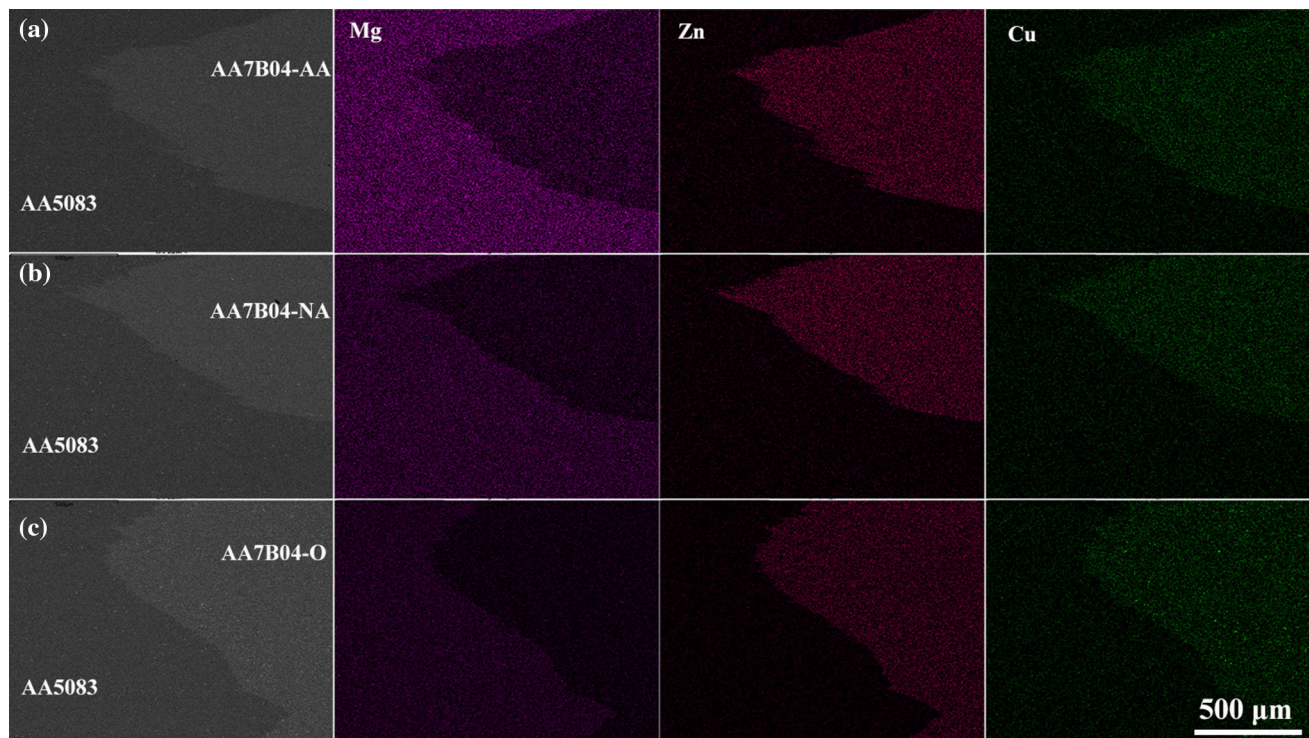


Fig. 4 SEM and EDS maps shown the difference in the alloying element contents in the SZ at the interface of (a) AA5083/AA7B04-AA, (b) AA5083/AA7B04-NA and (c) AA5083/AA7B04-O

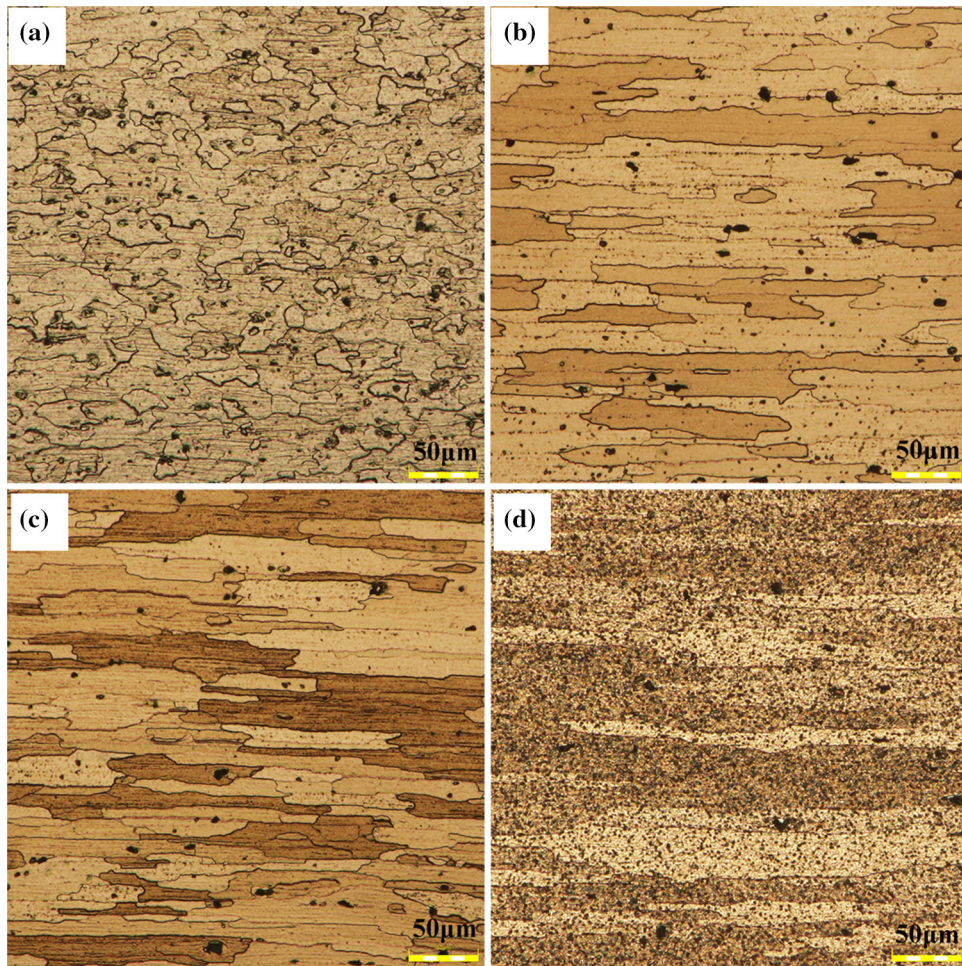


Fig. 5 OM micrographs of the BM (a) AA5083 and AA7B04 under (b) AA, (c) NA and (d) O states

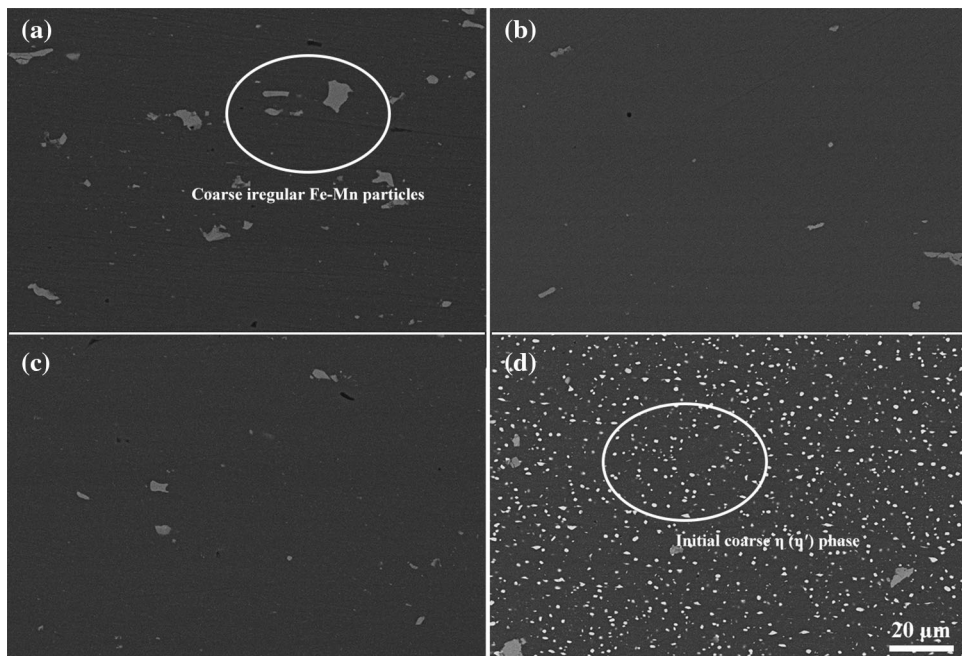


Fig. 6 Back-scattering electron (BSE) images of the second-phase particles (a) AA5083 BM and precipitates in the AA7B04 BM under (b) AA, (c) NA and (d) O states

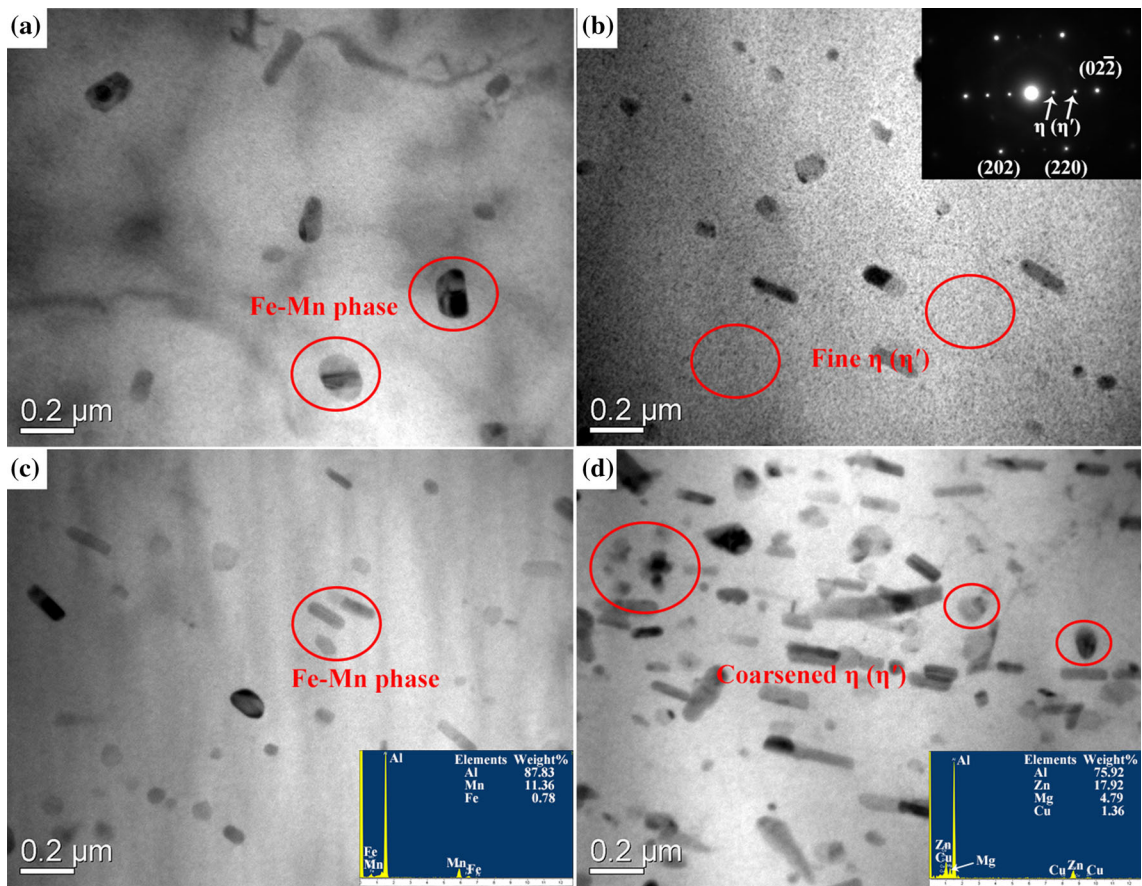


Fig. 7 TEM micrographs of the second-phase particles in the (a) AA5083 BM and precipitates in the AA7B04 BM under (b) AA, (c) NA and (d) O states

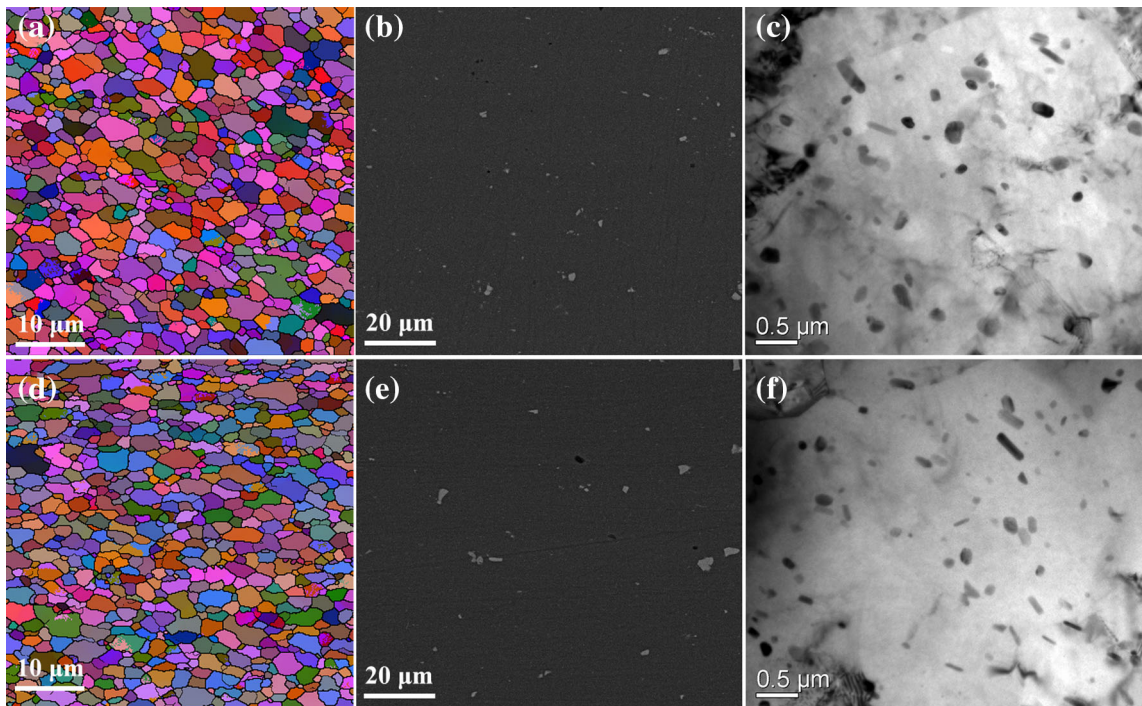


Fig. 8 EBSD grain boundary maps and the images of the second-phase particles analyzed by BSE and TEM in the SZ of (a)-(c) S-1 sample and (d)-(f) AA5083 side of D-1 sample

microstructural evolution in the SZ on the AA5083 side. The D-1 sample is selected to observe the microstructure of SZ on the AA5083 side. The grain size of D-1 is similar to that of S-1 sample (Fig. 8d), which is $1.9 \pm 0.1 \mu\text{m}$. Besides, the coarse irregular particles of D-1 on the AA5083 side are also broken, and the amount of fine particles is the same as that of similar FSW sample (Fig. 8e and f). The similar microstructure obtained in the SZ between similar and dissimilar FSW samples for AA5083 alloy indicates that the interference between AA5083 and AA7B04 is slight during FSW.

On the AA7B04 side, both the OM and TEM analyses (Fig. 9) indicate that the discrepancy in the grain size in the SZ under different initial base metal states is not significant. Moreover, the grain size of the SZ on the AA7B04 side is

similar to that on the AA5083 side. This is not surprising for the same level in grain size under all FSW conditions as the grain size after dynamic recrystallization (DRX) depends on the heat input (Ref 20). The same process parameter used in the present work leads to a similar heat input, and hence, the grain size in the SZ becomes similar. Different from the stable particles of AA5083 (Fig. 7a, 8c and f), the evolution of strengthening precipitates in AA7B04 is much more sensitive during FSW. On the AA7B04 side for both D-1 and D-2 samples (Fig. 10a and b), some coarsened precipitates are observed in the SZ, while the variation in the precipitates for D-3 samples is slight (Fig. 10c). Because of the different kinetics of dissolution/coarsening for the precipitates, the behavior of strengthening precipitates during FSW changes (Ref 8, 18, 21). For

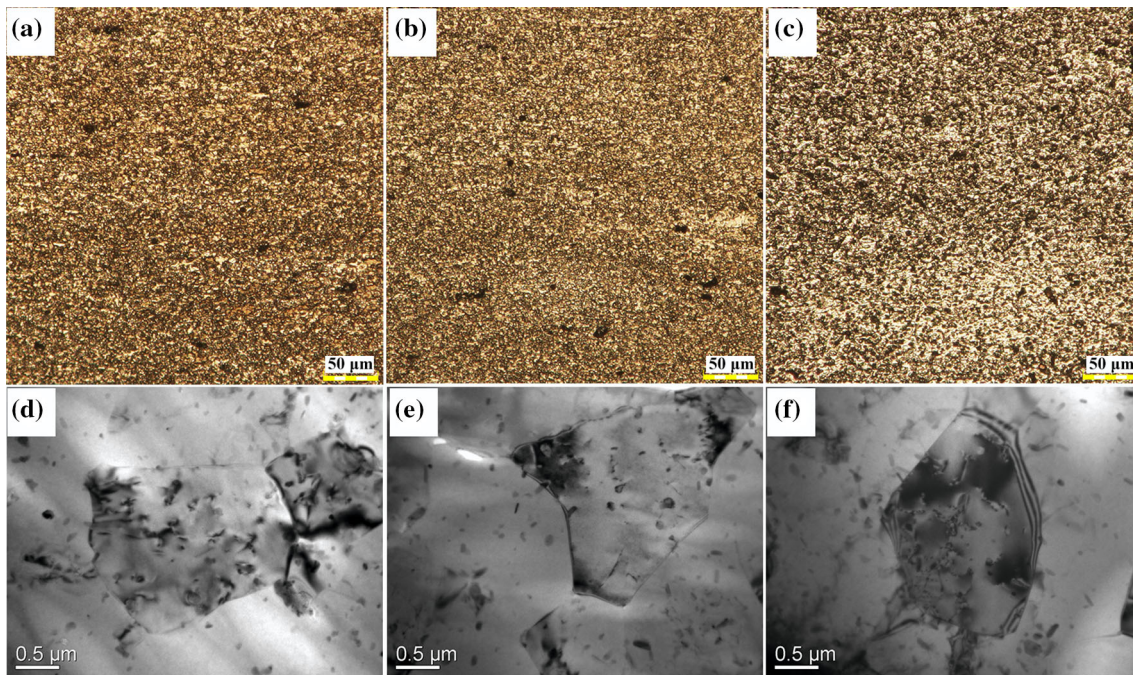


Fig. 9 Grains in the SZ on the AA7B04 side of D-1, D-2 and D-3 samples analyzed by OM (a)-(c) and TEM (d)-(f)

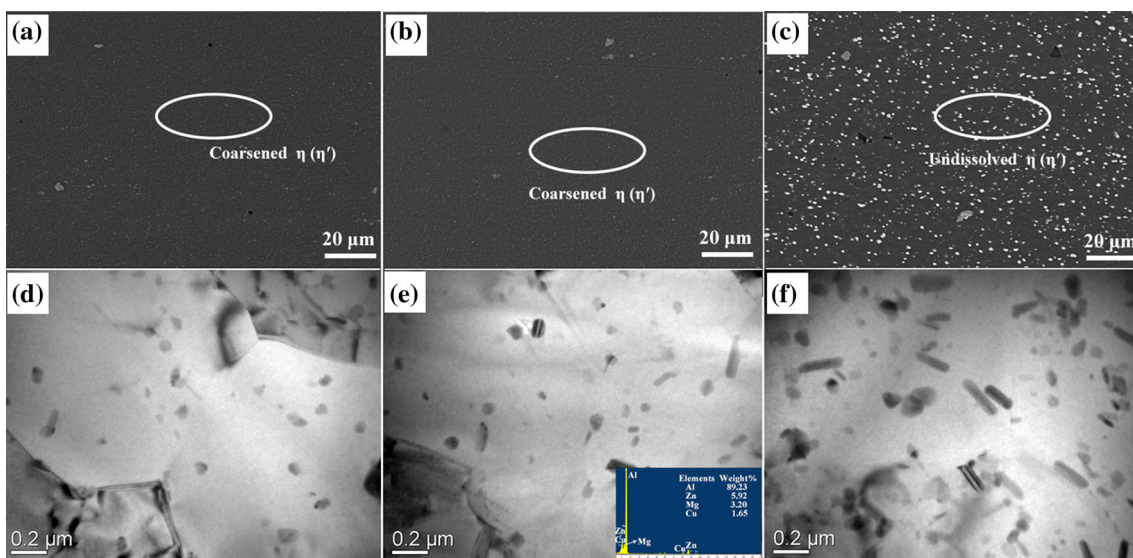


Fig. 10 Precipitates in the SZ on the AA7B04 side of dissimilar samples analyzed by BSE (a)-(c) and TEM (d)-(f)

AA7B04-AA (Fig. 10d), most of the initial fine η (η') phase dissolve on account of their high dissolution kinetics; meanwhile, some of the η (η') phase remains and get coarsened. Similarly, for AA7B04-NA (Fig. 10e), the GP zones dissolve entirely and only the coarsened η (η') phase remains. On the contrary, the initial η (η') phase in AA7B04 under O state is much coarser, which makes it difficult to dissolve within a relatively short FSW heat period, and most of the coarse η (η') phase remains (Fig. 10f).

3.3 Hardness Profiles

The hardness profiles measured across the cross section of joints using similar and dissimilar FSW are presented in Fig. 11. For S-1 sample, the hardness distribution is symmetric, and moreover, SZ is hardened a bit which mainly attributes to the grain refinement caused by the DRX. However, for the dissimilar FSW samples, due to the distinct mechanical properties of BM, an asymmetric hardness distribution profile is observed under all tested welding conditions. The variation of hardness on the AA5083 side of all dissimilar FSW joints is the same as that of S-1 sample, which is caused by the similar microstructure between similar and dissimilar FSWs for AA5083 as mentioned in section 3.2. By contrast, the variation of hardness distribution on the AA7B04 side is dependent on the initial base metal state. A significant softening is observed in the SZ on the 7B04 side for D-1 and D-2 samples, compared with the hardness of their corresponding BM. The formation of these soft regions is a consequence of coarsening/dissolution of strengthening precipitates (Ref 22). Differing from D-1 and D-2 samples, the SZ on the AA7B04 side for D-3 sample is strengthened, and the hardness of SZ for AA7B04-O alloy is twice than that of the BM under O state.

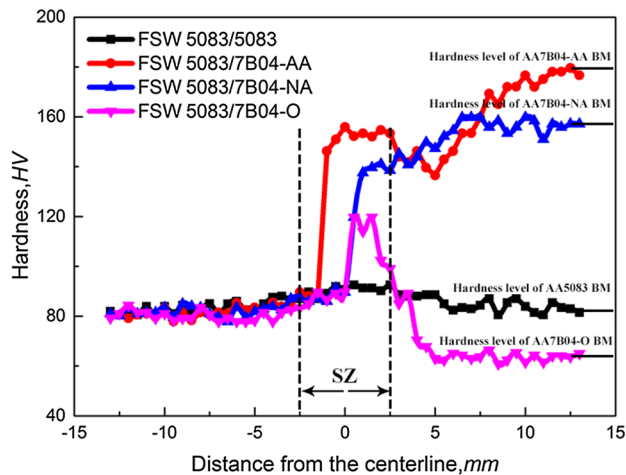


Fig. 11 Hardness distribution across the cross section of joints using different FSW conditions

During FSW process, high temperature (ranging from 400 to 500 °C) can be generated in the SZ (Ref 23), resulting in dissolution/coarsening of the strengthening precipitates on the AA7B04 side. For D-1 and D-2 samples (Fig. 10d and e), the initial fine η (η') phase or GP zones dissolved during FSW and the remaining η (η') phase are coarsened, which decreases the precipitation strengthening significantly. Furthermore, the increase in the strength by grain refinement cannot offset the strength decrease caused by precipitation strengthening (Ref 24, 25), resulting in the softening of SZ on the AA7B04 side. On the contrary, the precipitation strengthening of AA7B04-O before FSW is weak due to the existence of coarse precipitates. During FSW, few precipitates dissolve and the remaining precipitates keep coarse (Fig. 10f), and hence, the loss in precipitation strengthening caused by FSW is nonsignificant. The improvement in the hardness of SZ on the AA7B04-O side is mainly attributed to the grain refinement strengthening.

3.4 Tensile Properties

The results of the tensile tests are listed in Table 4. The stress-strain diagram of FSW samples is shown in Fig. 12; besides, the failure location of FSW samples was also presented (as shown in Fig. 13). For similar FSW sample S-1, the joints are failed in the SZ and the joint efficiency for the ultimate tensile strength is found to be only 89% that of AA5083 BM. However, based on the result of hardness, the SZ is hardened and the joints should not be fractured in the SZ on account of its high hardness. The contradiction between the softened tensile strength and strengthened hardness is supposed mainly caused by the zigzag line and kissing bond defects in the SZ. During tensile tests, a crack may relatively easily nucleate at these defects and propagate along its trajectory (Ref 12). This process

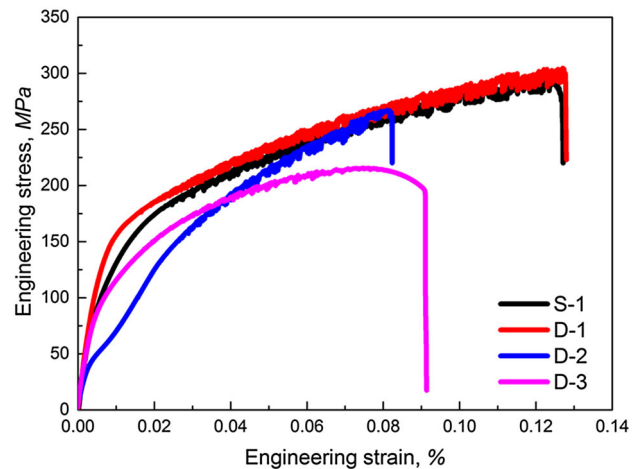


Fig. 12 Deformation diagrams showing tensile behavior of material produced by FSW

Table 4 Tensile properties of similar and dissimilar FSW samples

| Sample | Yield strength, MPa | Ultimate tensile strength, MPa | Elongation, % | Failure location |
|--------|---------------------|--------------------------------|---------------|------------------|
| S-1 | 146 ± 5 | 285 ± 15 | 10.0 ± 0 | SZ |
| D-1 | 161 ± 5 | 305 ± 5 | 10.5 ± 1 | BM of AA5083 |
| D-2 | 154 ± 3 | 280 ± 15 | 5.0 ± 0.5 | SZ |
| D-3 | 127 ± 7 | 218 ± 2 | 9.0 ± 0.3 | BM of AA7B04-O |

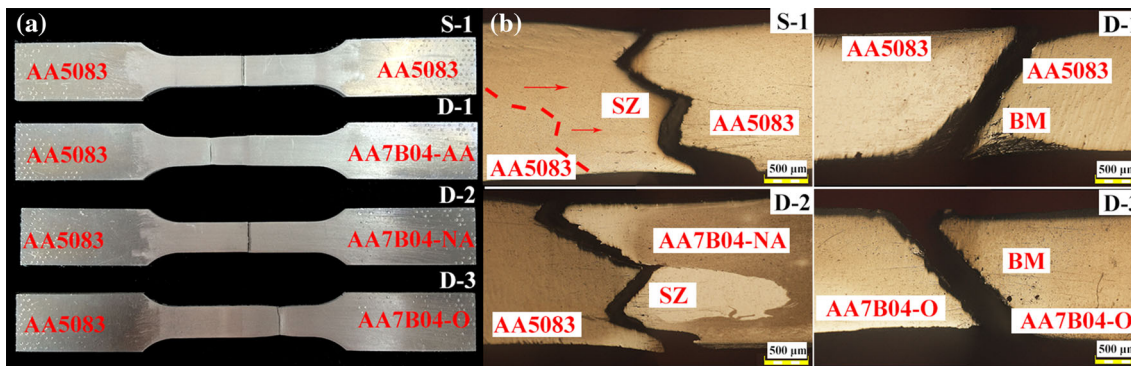


Fig. 13 Fractography of the tested samples produced by FSW (a) photographic and (b) optical images

may deteriorate not only the tensile strength of SZ but also the ductility of the FSW joints. To avoid this problem, the use of a relatively high rotational speed is recommended.

For dissimilar FSW samples, the joints fail in the following location: (i) SZ, (ii) BM of AA5083 and (iii) BM of AA7B04-O. This is not a surprise that D-1 sample fails in BM of AA5083, because the hardness of AA5083 BM is the lowest in the AA5083/AA7B04-AA joints, and the specimens always neck and fail within this weakest location. The same explanation can be used for D-3 sample that the FSW joints fail in the BM of AA7B04-O. Besides, the elongation of both D-1 and D-3 samples is lower than that of their corresponding BM. This is due to the fact that about half of the transverse specimen extracted from the joints consists of higher strength materials, and these sections of the specimen do not yield during testing, decreasing the ductility of the tensile specimen (Ref 26). Differently, for D-2 sample, the joints fail in the SZ, regardless of the high hardness of SZ. In addition, the ductility of D-2 sample is relatively low. This strange fracture mode supposes to be mainly caused by the undetected voids in the SZ. It is always difficult to observe these voids which are discontinuous along the welding directions (Ref 6). Based on our previous study (Ref 27), a second or third overlapping FSW/FSP pass could repair these voids, and furthermore, the mechanical properties of the materials are essentially unchanged. A second FSW pass is applied to D-2 sample in the present work, and it is found that the failure location of joints shifts from SZ to BM of AA5083. Therefore, it can be inferred that the strange fracture mode of D-2 sample is attributed to the undetected voids.

4. Conclusions

The microstructure and mechanical properties of dissimilar friction stir-welded AA5083-AA7B04 butt joint were analyzed, and the following results were obtained:

1. Compared with the joints placing hard alloy (AA7B04-AA or AA7B04-NA) on the RS, it became easier transporting AA5083 from AS to RS when placed the soft alloy (AA7B04-O) on the RS. Besides, there was no atomic diffusion at the interface of AA5083/AA7B04, and the mixing of the two materials was merely mechanical.
2. Both AA5083 and AA7B04 alloys had experienced DRX, and the grain size in the SZ decreased significantly. The evolution of second-phase particles in

AA5083 during dissimilar FSW was relatively simple: The coarse irregular particles were broken. The behavior of strengthening precipitates of AA7B04 during dissimilar FSW became much more complex compared with that of AA5083. For AA7B04-AA and AA7B04-NA, the initial fine η (η') phase or GP zones dissolved, while the dissolution of the initial precipitates η (η') was negative for AA7B04 under O state.

3. Due to the different initial base metal states, the variation in hardness after dissimilar FSW was different. For the joints of AA5083/AA7B04-AA and AA5083/AA7B04-NA, AA5083 exhibited certain hardness increase in the SZ compared to its corresponding BM because of the grain refinement. However, the hardness in the SZ on AA7B04-AA and AA7B04-NA side decreased on account of the loss of the precipitation strengthening. The low hardness region was the AA5083 BM. By contrast, for the joints of AA5083/AA7B04-O, an enhancement in hardness of the SZ on both sides was observed, and the minimum hardness values were observed in BM of AA7B04-O.
4. Two kinds of failure locations were observed, with one through the soft material BM side and the other through the SZ. The sound joints (AA5083/AA7B04-AA and AA5083/AA7B04-O) failed in the BM on the soft material side, which corresponded very well to the minimum values in hardness profiles. The joints (AA5083/AA5083 and AA5083/AA7B04-O) failed in the SZ were attributed to the defect such as "zigzag line," kissing bond and discontinuous voids.

Acknowledgments

One of the authors (Zihui CAI) gratefully acknowledges support from the National Science Foundation for Young Scientists of China (No: 51501035) and Chinese Postdoctoral Science Foundation (2016T90227).

References

1. R.S. Mishra and Z.Y. Ma, Friction Stir Welding and Processing, *Mater. Sci. Eng. R*, 2005, **50**(1-2), p 1-78
2. G.R. Cui, Z.Y. Ma, and S.X. Li, Periodical Plastic Flow Pattern in Friction Stir Processed Al-Mg Alloy, *Scripta Mater.*, 2008, **58**(12), p 1082-1085

3. H.J. Liu and X.L. Feng, Effect of Post-Processing Heat Treatment on Microstructure and Microhardness of Water-Submerged Friction Stir Processed 2219-T6 Aluminum Alloy, *Mater. Des.*, 2013, **47**, p 101–105
4. H. Robe, Y. Zedan, J. Chen, H. Monajati, E. Feulvarch, and P. Bocher, Microstructural and Mechanical Characterization of a Dissimilar Friction Stir Welded Butt Joint Made of AA2024-T3 and AA2198-T3, *Mater. Charact.*, 2015, **110**, p 242–251
5. J.F. Guo, H.C. Chen, C.N. Sun, G. Bi, Z. Sun, and J. Wei, Friction Stir Welding of Dissimilar Materials Between AA6061 and AA7075 Al Alloys Effects of Process Parameters, *Mater. Des.*, 2004, **56**, p 185–192
6. R.I. Rodriguez, J.B. Jordon, P.G. Allison, T. Rushing, and L. Garcia, Microstructure and Mechanical Properties of Dissimilar Friction Stir Welding of 6061-to-7050 Aluminum Alloys, *Mater. Des.*, 2015, **83**, p 60–65
7. R. Palanivel, P.S. Mathews, N. Murugan, and I. Dinaharan, Effect of Tool Rotational Speed and Pin Profile on Microstructure and Tensile Strength of Dissimilar Friction Stir Welded AA5083-H111 and AA6351-T6 Aluminum Alloys, *Mater. Des.*, 2012, **40**, p 7–16
8. Y. Chen, H. Ding, Z. Cai, J. Zhao, and J. Li, Effect of Initial Base Metal Temper on Microstructure and Mechanical Properties of Friction Stir Processed Al-7B04 Alloy, *Mater. Sci. Eng. A*, 2016, **650**, p 396–403
9. G.R. Cui, Z.T. Ma, and S.X. Li, The Origin of Non-Uniform Microstructure and Its Effects on the Mechanical Properties of a Friction Stir Processed Al-Mg Alloy, *Acta Mater.*, 2009, **57**(19), p 5718–5729
10. H.L. Hao, D.R. Ni, H. Huang, D. Wang, B.L. Xiao, Z.R. Nie, and Z.Y. Ma, Effect of Welding Parameters on Microstructure and Mechanical Properties of Friction Stir Welded Al-Mg-Er Alloy, *Mater. Sci. Eng. A*, 2013, **559**, p 889–896
11. S. Malopheyev, V. Kulitskiy, S. Mironov, D. Zhemchuzhnikova, and R. Kaibyshev, Friction-Stir Welding of an Al-Mg-Sc-Zr Alloy in as-Fabricated and Work-Hardened Conditions, *Mater. Sci. Eng. A*, 2014, **600**, p 159–170
12. Y.S. Sato, H. Takauchi, S.H.C. Park, and H. Kokawa, Characteristics of the Kissing-Bond in Friction Stir Welded Al Alloy 1050, *Mater. Sci. Eng. A*, 2005, **405**, p 333–338
13. M.A. Sutton, B. Yang, A.P. Reynolds, and R. Taylor, Microstructural Studies of Friction Stir Welds in 2024-T3 Aluminum, *Mater. Sci. Eng. A*, 2002, **323**(1-2), p 160–166
14. Y. Tao, Z. Zhang, D.R. Ni, D. Wang, B.L. Xiao, and Z.Y. Ma, Influence of Welding Parameter on Mechanical Properties and Fracture Behavior of Friction Stir Welded Al-Mg-Sc Joints, *Mater. Sci. Eng. A*, 2014, **612**, p 236–245
15. K. Chen, W. Gan, K. Okamoto, K. Chung, and R.H. Wagoner, The Mechanism of Grain Coarsening in Friction-Stir-Welded AA5083 After Heat Treatment, *Metall. Mater. Trans. A*, 2011, **42**(2), p 488–507
16. J.-Q. Su, T.W. Nelson, R. Mishra, and M. Mahoney, Microstructural Investigation of Friction Stir Welded 7050-T651 Aluminum, *Acta Mater.*, 2003, **51**(3), p 713–729
17. K. Stiller, P.J. Warren, V. Hansen, J. Angenete, and J. Gannes, Investigation of Precipitation in an Al-Zn-Mg Alloy After Two-Step Aging Treatment at 100 and 150 °C, *Mater. Sci. Eng. A*, 1999, **270**(1), p 55–63
18. X.J. Jiang, J. Tafto, B. Noble, B. Holme, and G. Waterloo, Differential Scanning Calorimetry and Electron Diffraction Investigation on Low-Temperature Aging in Al-Zn-Mg Alloys, *Metall. Mater. Trans. A*, 2000, **31**(2), p 339–348
19. C.B. Fuller, M.W. Mahoney, M. Calabrese, and L. Micono, Evolution of Microstructure and Mechanical Properties in Naturally Aged 7050 and 7075 Al Friction Stir Welds, *Mater. Sci. Eng. A*, 2010, **527**(9), p 2233–2240
20. Y.J. Kwon, N. Saito, and I. Shigematsu, Friction Stir Process as a New Manufacturing Technique of Ultrafine Grained Aluminum Alloy, *J. Mater. Sci. Lett.*, 2002, **21**(19), p 1473–1476
21. J. Yan and A.P. Reynolds, Effect of Initial Base Metal Temper on Mechanical Properties in AA7050 Friction Stir Welds, *Sci. Technol. Weld. Join.*, 2009, **14**(4), p 282–287
22. C. Sharma, D.K. Dwivedi, and P. Kumar, Influence of Pre-Weld Temper Conditions of Base Metal on Microstructure and Mechanical Properties of Friction Stir Weld Joints of Al-Zn-Mg Alloy AA7039, *Mater. Sci. Eng. A*, 2015, **650**, p 107–109
23. Y. Chen, H. Ding, J. Li, J. Zhao, M. Fu, and X. Li, Effect of Welding Heat Input and Post-Welded Heat Treatment on Hardness of Stir Zone for Friction Stir-Welded 2024-T3 Aluminum Alloy, *Trans. Nonferr. Met. Soc.*, 2015, **25**(8), p 2524–2532
24. X. Feng, H. Liu, and S.S. Babu, Effect of Grain Size Refinement and Precipitation Reactions on Strengthening Friction Stir Processed Al-Cu Alloys, *Scripta Mater.*, 2011, **65**(12), p 1057–1060
25. J. Zander and R. Sandstrom, One Parameter Model for Strength Properties of Hardenable Aluminum Alloys, *Mater. Des.*, 2008, **29**(8), p 1540–1548
26. G. Ipekoglu and G. Cam, Effects of Initial Temper Condition and Postweld Heat Treatment on the Properties of Dissimilar Friction-Stir-Welded Joints Between AA7075 and AA6061 Aluminum Alloys, *Metall. Mater. Trans. A*, 2014, **45**(7), p 3074–3087
27. Y. Chen, H. Ding, J. Li, Z. Cai, J. Zhao, and W. Yang, Influence of Multi-Pass Friction Stir Processing on the Microstructure and Mechanical Properties of Al-5083 Alloy, *Mater. Sci. Eng. A*, 2016, **650**, p 281–289